Nanoscale

PAPER

Cite this: *Nanoscale*, 2014, **6**, 14453

Novel chemical route for atomic layer deposition of MoS_2 thin film on SiO_2/Si substrate†

Zhenyu Jin,‡ Seokhee Shin,‡ Do Hyun Kwon, Seung-Joo Han and Yo-Sep Min*

Received 20th August 2014,
Accepted 13th October 2014

DOI: 10.1039/c4nr04816d

www.rsc.org/nanoscale

Recently MoS_2 with a two-dimensional layered structure has attracted great attention as an emerging material for electronics and catalysis applications. Although atomic layer deposition (ALD) is well-known as a special modification of chemical vapor deposition in order to grow a thin film in a manner of layer-by-layer, there is little literature on ALD of MoS_2 due to a lack of suitable chemistry. Here we report MoS_2 growth by ALD using molybdenum hexacarbonyl and dimethyldisulfide as Mo and S precursors, respectively. MoS_2 can be directly grown on a SiO_2/Si substrate at 100 °C *via* the novel chemical route. Although the as-grown films are shown to be amorphous in X-ray diffraction analysis, they clearly show characteristic Raman modes (E^1_{2g} and A_{1g}) of 2*H*-MoS_2 with a trigonal prismatic arrangement of S–Mo–S units. After annealing at 900 °C for 5 min under Ar atmosphere, the film is crystallized for MoS_2 layers to be aligned with its basal plane parallel to the substrate.

1 Introduction

Due to the success in recent research on graphene and its various applications,[1] two-dimensional (2D) materials such as transition metal dichalcogenides (TMDs) have attracted great attention in academia and industry.[2,3] Among the TMDs (MX_2), where M is a transition metal of groups 4–10 and X is a chalcogen, MoS_2 is one of the potential materials for electronics and catalysis applications.[4,5] While bulk MoS_2 is an n-type semiconductor with an indirect bandgap (~1.3 eV), the atomic monolayer of MoS_2 has a direct bandgap (~1.8 eV).[6] Several groups have reported performance of MoS_2 in field effect transistors and logic devices in which a monolayer or a film of MoS_2 was used as a semiconducting channel in the transistor, instead of silicon.[7–9] In addition, MoS_2 is a strong candidate to replace expensive Pt catalyst in the electrochemical hydrogen evolution reaction (HER) for renewable H_2 production.[10,11]

For the electronic device applications of 2D materials, they should have a bandgap to ensure a high on/off ratio of the transistor, and should be directly grown with a high crystallinity on an insulating material (*e.g.*, SiO_2). However, since graphene has intrinsically no bandgap and cannot be grown without a catalytic film (*e.g.*, Ni and Cu), the performance of the graphene transistor is not as excellent as expected from theoretical calculations and the best experimental mobility (10^5 cm^2 V^{-1} s^{-1}) was obtained by using an exfoliated graphene.[12] It was recently reported that a monolayer or ultrathin film of MoS_2 could be directly grown on an insulator without any catalyst by chemical vapor deposition (CVD).[13–16] However, a common problem of CVD methods is that elemental sulfur is used as a sulfur precursor for MoS_2 CVD. The vapor pressure of elemental sulfur is ~10^{-5} Torr at 40 °C, which is much lower in comparison to typical vapor pressures of CVD precursors.[17] Even though large-area MoS_2 monolayers were demonstrated by the CVD method, it cannot be utilized in mass production due to a lack of reliability and reproducibility of the process.

On the other hand, atomic layer deposition (ALD) is a special modification of CVD for growing a thin film *via* a self-limiting mechanism.[18] In CVD, while two precursors (*e.g.*, Mo and S precursors) are simultaneously supplied to a substrate, they are alternately exposed onto the substrate and subsequently purged for each precursor in ALD. Therefore one ALD cycle generally consists of two half reactions, which are achieved by repeating four steps (the first precursor exposure and purging steps for the first half reaction and the second precursor exposure and purging steps for the second half reaction). In addition, growth temperature in ALD is maintained to be low enough in order to avoid thermal decomposition of the precursors. Consequently, the film grows with the number of ALD cycles *via* chemisorption of each precursor, which occurs in turn repeatedly. Considering the principle of ALD being based on chemisorption, it is expected that ALD may be an excellent tool for preparing layered MoS_2.

Recently, a MoO_3 thin film was grown by ALD using molybdenum hexacarbonyl ($Mo(CO)_6$) and various oxidants.[19] ALD of

Department of Chemical Engineering, Konkuk University, 120 Neungdong-Ro, Gwangjin-Gu, Seoul 143-701, Korea. E-mail: ysmin@konkuk.ac.kr

† Electronic supplementary information (ESI) available: XPS depth profiles for the as-grown and the annealed MoS_2 films. See DOI: 10.1039/c4nr04816d

‡ These authors equally contributed to this work.

a Mo thin film was also reported by using MoF_6 and Si_2H_6.[20] A MoS_2 HER catalyst was prepared by sulfurizing a MoO_3 thin film, which was grown by ALD from $Mo(CO)_6$ and ozone.[21] Very recently, the first report on ALD of MoS_2 was presented by Loh *et al.* by using $MoCl_5$ and H_2S on sapphire substrates.[22] To the best of our knowledge, this is the only paper for MoS_2 ALD ever reported, due to a lack of suitable chemistry for ALD. Here we present a novel chemical route for MoS_2 ALD in which MoS_2 can be directly grown on a SiO_2/Si substrate using $Mo(CO)_6$ and dimethyldisulfide (CH_3SSCH_3, DMDS) as Mo and S precursors, respectively.

2 Experimental

In order to investigate the growth behavior of MoS_2 using the novel chemistry of ALD, thin films were simultaneously grown on both SiO_2 (300 nm)/Si (1 × 1 or 2 × 2 cm^2) and bare Si wafers in a laminar flow type ALD reactor. The films grown on the bare Si were used to measure the thickness by spectroscopic ellipsometry (SE). $Mo(CO)_6$ and DMDS (Aldrich) were vaporized from external canisters at room temperature and led into the reactor through solenoid valves with a carrier gas of N_2 (100 sccm, 99.999%) for $Mo(CO)_6$ and without any carrier gas for DMDS. The doses of $Mo(CO)_6$ and DMDS were $\sim 1.8 \times 10^{-6}$ and $\sim 4.0 \times 10^{-4}$ mol s^{-1}, respectively. For purging the reactor, N_2 gas was used with a flow rate of 300 sccm. All delivery lines were maintained at 80 °C. The growth temperature was controlled by using a lamp heater, and monitored with a thermocouple which was closely placed to the specimen. The base pressure of the reactor was less than 10 mTorr and ALD was processed at a working pressure range of 1.4–3.3 Torr.

All thicknesses of the grown films were measured by SE (MG-1000, NanoView). The incident angle of the polarized light in the SE was fixed at around 70°, and the incident light has a spectral range of 1.5–5.0 eV. The measured data by SE was fitted with a Tauc–Lorentz dispersion function in order to determine the thickness.[23] Raman spectroscopy (Alpha 500R, WiTec) was used to characterize MoS_2 films using a 532 nm laser excitation. The Si peak at 521 cm^{-1} was used as a reference for wavenumber calibration. X-ray photoelectron spectroscopic (XPS) spectra were obtained on a PHI 5000 Versaprobe (ULVAC PHI) using monochromatic Al Kα emission. Binding energies were measured using the C 1s peak (284.8 eV) of the adventitious carbon as an internal standard. X-ray diffraction (XRD) measurements were carried out in $\theta/2\theta$ scan mode using a Philips X'pert Pro MRD X-ray diffractometer with Cu Kα emission. The high resolution transmission electron microscopy (HR-TEM) sample was prepared by using a focused ion beam and its microstructure was imaged in a TITAN TM 80-300 FEI microscope.

3 Results and discussion

3.1 Self-limiting growth of MoS_2 thin film by ALD

Although $Mo(CO)_6$ is a solid at ambient condition, it has a vapor pressure of 0.10–0.15 Torr at room temperature, which is enough for deposition process in vacuum.[24,25] Several groups have used $Mo(CO)_6$ as a Mo precursor in ALD or CVD of MoO_3 thin films.[19,26,27] It is well known that physisorbed $Mo(CO)_6$ undergoes decarbonylation to form chemisorbed subcarbonyls, $Mo(CO)_n$ ($n \leq 5$), on the surface of various substrates.[28–31] Therefore $Mo(CO)_6$ was chosen as a Mo precursor for the first-half reaction of ALD.

Chemisorption of organosulfur compounds (*e.g.*, DMDS) has been intensively studied due to their importance in hydrodesulfurization catalysis, self-assembled monolayers and so on.[32,33] There are several reports for dissociative chemisorption of DMDS through S–S bond cleavage to form methylthiolate intermediate (CH_3S–) on the surface of various substrates.[32–36] The surface methylthiolates can undergo additional decomposition *via* C–S bond cleavage to produce sulfur adatoms releasing gaseous molecules such as $(CH_3)_2S$ and CH_3CH_3. This reaction is utilized in thiol desulfurization by using Mo, sulfided Mo, or $Mo(CO)_6$ catalysts.[33] Because it is expected that the formation of surface S atoms from the methylthiolates may be also catalyzed by the chemisorbed $Mo(CO)_n$, DMDS was selected as a S precursor for the second-half reaction of ALD. As a result, the chemistry for our MoS_2 ALD may consist of the first- and second-half reactions given in eqn (1) and (2):

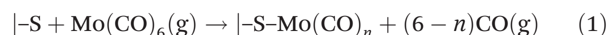

$$|\text{–S} + \text{Mo(CO)}_6(\text{g}) \rightarrow |\text{–S–Mo(CO)}_n + (6-n)\text{CO(g)} \quad (1)$$

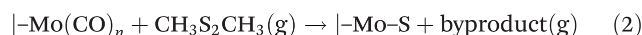

$$|\text{–Mo(CO)}_n + \text{CH}_3\text{S}_2\text{CH}_3(\text{g}) \rightarrow |\text{–Mo–S} + \text{byproduct(g)} \quad (2)$$

where |– denotes surface.

In order to confirm the self-limiting chemisorption of the precursors in each half-reaction, thicknesses of the films grown at 100 °C for 100 cycles were plotted against exposure times of $Mo(CO)_6$ and DMDS, shown in Fig. 1. The chemisorption of $Mo(CO)_6$ in the first-half reaction (Fig. 1a) shows the typical self-limiting growth at exposure times (x) of $Mo(CO)_6$ longer than 3 s due to the saturation of adsorption sites occupied by $Mo(CO)_n$. Similarly, DMDS also follows the self-limiting growth mechanism as shown in Fig. 1b, however the thickness saturates in a much shorter exposure time (y) owing

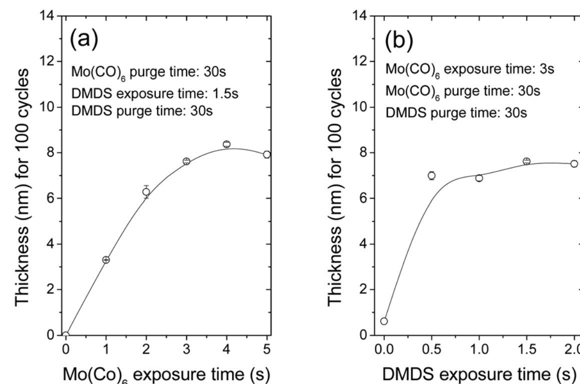

Fig. 1 Thicknesses of MoS_2 films against exposure times of $Mo(CO)_6$ (a) and DMDS (b). ALD was performed at 100 °C for 100 cycles. The curves are drawn for guiding the eye.

 This journal is © The Royal Society of Chemistry 2014

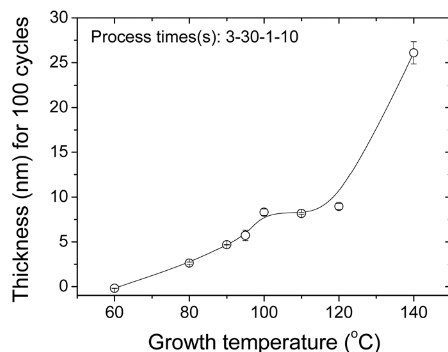

Fig. 2 Thickness of MoS_2 films against growth temperature. ALD was performed for 100 cycles with the process times given in the figure. The curves are drawn for guiding the eye.

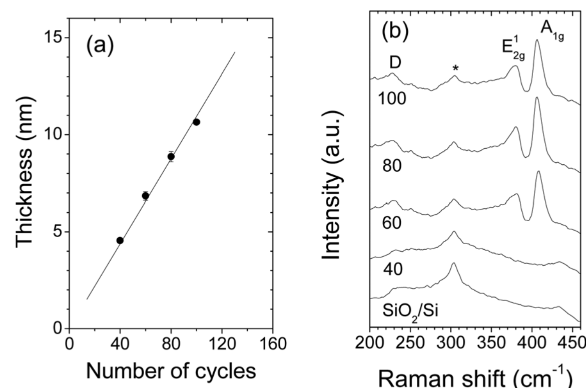

Fig. 3 (a) Thickness of MoS_2 films against number of ALD cycles. (b) Raman spectra (532 nm laser excitation) of MoS_2 films that were grown for various numbers of ALD cycles (the numbers on each spectrum). ALD was performed on SiO_2/Si at 100 °C (x = 4 s and y = 1.5 s).

to its high vapor pressure (~29 Torr at room temperature).[37] In addition, when one of both half-reactions was performed with only one precursor by making the exposure time of the other precursor be zero, the thickness increase by a deposit was negligible as shown with the thicknesses at $x = 0$ (Fig. 1a) or $y = 0$ (Fig. 1b). Consequently, we can exclude the possibility of uncontrolled thermal decomposition of both precursors in the film growth. It should be noted that when only DMDS was exposed without the exposure of $Mo(CO)_6$ (*i.e.*, $x = 0$), the thickness of the deposit was also zero. However when the DMDS was exposed on the surface $Mo(CO)_n$ (*i.e.*, $x > 0$), the film can grow as shown in Fig. 1a. This is evidence that reveals that the decomposition of the methylthiolate *via* C–S bond cleavage is also catalyzed by $Mo(CO)_n$, as done by $Mo(CO)_6$.[33]

Generally, film growth by ALD shows a particular temperature window in which the growth-per-cycle (GPC) is weakly dependent on the growth temperature.[18] Fig. 2 shows the film thicknesses grown for 100 cycles (x = 3 s and y = 1 s) at different temperatures. Film growth is negligible at 60 °C. However, as the growth temperature becomes higher, the film thickness increases with the growth temperature and then saturates at 100 °C. The typical plateau of the GPC is observed in a temperature range of 100–120 °C. ALD process at higher temperatures than 120 °C results in a rapid increase of the GPC due to the uncontrolled thermal decomposition of precursors.

In addition, due to the self-limiting nature of ALD, the film thickness linearly increases with the number of ALD cycles. This is a great advantage of ALD because the thickness of the film can be controlled on an angstrom scale by the number of ALD cycles with a value of GPC. Fig. 3a shows thicknesses of MoS_2 films against the number of ALD cycles. The GPC of MoS_2 at 100 °C was evaluated to be 0.11 ± 0.01 nm per cycle (when x = 4 s and y = 1.5 s) from the slope in the figure.

3.2 Characterization of MoS_2 thin film grown by ALD

Since the temperature window for our ALD chemistry is very low for the film to be crystallized, the films grown in this temperature range (100–120 °C) are shown to be amorphous by TEM and XRD analysis (see Fig. 5b and 6). If the ALD MoS_2 films were completely amorphous, no clear peaks should be visible in Raman spectra.[38] However the Raman spectra in Fig. 3b reveal that the amorphous MoS_2 film grown on SiO_2/Si has a locally-ordered S–Mo–S unit with an atomic arrangement of 2H-MoS_2. In the 2H structure of molybdenite (naturally occurring MoS_2), an atomic plane of Mo is sandwiched between two atomic planes of S in a trigonal prismatic arrangement. For the bulk MoS_2, the characteristic E^1_{2g} (in-plane) and A_{1g} (out-of-plane) Raman modes appear at 383 and 408 cm^{-1}, respectively.[39,40]

The ALD MoS_2 films grown with more than 60 ALD cycles clearly show the characteristic E^1_{2g} mode at 381 cm^{-1} and the A_{1g} mode at 406 cm^{-1}. However the film grown for 40 cycles does not show any MoS_2 peak as compared with the Raman spectrum of the SiO_2/Si substrate (the Si peak at 304 cm^{-1} is marked with an asterisk in Fig. 3b). The E^1_{2g} and A_{1g} peaks also show a significant red-shift of 2 cm^{-1} and broadening of the characteristic modes compared to the bulk MoS_2. While the bulk or few-layered MoS_2 generally show a line width (full width at half maximum, FWHM) range of 2–6 cm^{-1} for both peaks,[40] the FWHM of ALD MoS_2 films (12–14 cm^{-1}) is much broader. It is possibly due to the locally-ordered microstructure. Recently, it has been reported that the E^1_{2g} and A_{1g} peaks can be shifted down and broadened for nanoparticles.[11,41,42]

Generally, the number of S–Mo–S layers in MoS_2 can be determined from the wavenumber difference (Δ) between E^1_{2g} and A_{1g} peaks, because the frequency of the former decreases and that of the latter increases with the number of layers.[40] For MoS_2 films with a higher number of layers than 5–6 layers, the Δ values are around 25 cm^{-1}. Even though the as-grown film by ALD does not show the layered crystalline structure in TEM and XRD analyses, since the thicknesses of the as-grown MoS_2 films with Raman peaks are thicker than 6 nm, the Δ values of them are also around 25 cm^{-1} as expected.

One more concern for the Raman spectra is the broad peak at 227 cm^{-1} marked with D in Fig. 3b. Although there is no Raman active mode for crystalline MoS_2 in the wavenumber region,[39] the D peak appears only when the E^1_{2g} and A_{1g} peaks

This journal is © The Royal Society of Chemistry 2014

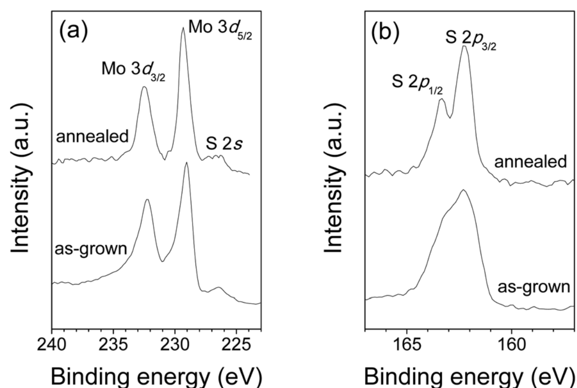

Fig. 4 XPS spectra of MoS_2 films as-grown by ALD or annealed at 900 °C for 5 min: Mo 3d (a) and S 2p (b) peaks. The binding energies were calibrated by using the C 1s peak (284.8 eV) of the adventitious carbon as an internal standard.

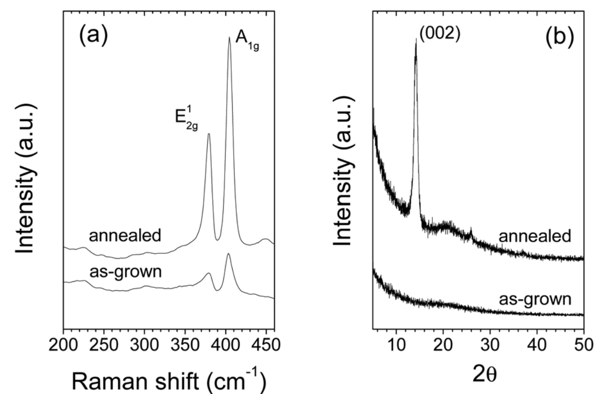

Fig. 5 Raman spectra (a) and XRD patterns (b) of MoS_2 films as-grown by ALD or annealed at 900 °C for 5 min.

are observed. Raman inactive modes due to the Raman selection rule can be activated when the crystal symmetry is broken by defects.[41,42] We believe that the D peak may be attributed to the disorder in the microstructure of MoS_2 film. This behavior seems to be analogous to the disorder-induced mode found in graphitic carbon materials.[43,44] Similar results were also reported in deposited MoS_2 films by pulsed laser deposition.[45] They found that the intensity of the disorder peak (D) was relatively attenuated compared to the intensity of the A_{1g} peak by annealing the samples because the crystallinity was improved.

The as-grown MoS_2 film was also characterized by X-ray photoelectron spectroscopy (XPS) as shown in Fig. 4. The spectra were obtained on the surface sputtered by 2 keV Ar^+ for 3 s in order to remove the adventitious carbon. The characteristic binding energies of Mo $3d_{3/2}$ and $3d_{5/2}$, which are attributed to Mo^{4+}, were observed at 232.3 and 229.1 eV, respectively.[38,46] For the binding energies of S $2p_{1/2}$ and $2p_{3/2}$ for divalent sulfide ion (S^{2-}), the $2p_{3/2}$ peak was observed at 162.3 eV, and the $2p_{1/2}$ peak was not clearly resolved but appeared as a shoulder of the $2p_{3/2}$ peak. These binding energy values are consistent with the previous reports for MoS_2.[38,46] However the stoichiometric ratio of S/Mo is estimated to be 1.21 for the as-grown film, possibly due to partial oxidation of the surface. Indeed, high oxygen content is detected on the surface with an O/S ratio of 0.85 while the carbon content is negligible (~0.1 at%). Furthermore, the oxygen concentration in the as-grown film rapidly decreases during XPS depth profiling (see Fig. S1 in ESI†). This supports the partial oxidation of the surface due to vulnerable nature of the as-grown film in air.

In order to crystallize the amorphous MoS_2, the as-grown film was annealed at 900 °C for 5 min under Ar atmosphere. The XPS spectra of the annealed film are also shown in Fig. 4. The Mo $3d_{3/2}$ and $3d_{5/2}$ peaks are located at 232.5 and 229.3 eV, respectively, and the S 2p doublet is clearly resolved at 163.3 and 162.2 eV after the annealing. In addition, the stoichiometric ratio of S/Mo is 2.01 and neither oxygen nor carbon atoms are detected on the annealed film.

After the annealing, the Raman modes become much stronger and narrower (FWHM ~9 cm^{-1}), compared with the as-grown film (Fig. 5a). The D peak at 227 cm^{-1}, originated from the disorder of MoS_2, is also relatively attenuated compared with that of the as-grown film. But the Δ value was not changed due to its 15 nm-thick thickness. For the same specimen, we investigated the crystal structure by XRD and high resolution TEM. The strong peak (2θ = 14.27) in Fig. 5b is attributed to (002) basal planes, for which interplanar spacing (d_{002}) is calculated to be ~0.625 nm from the 2θ value. This indicates a little expansion (~1.7%) of the layer spacing in comparison to that (0.615 nm) of molybdenite.[47] The cross-sectional high resolution TEM image (Fig. 6) also shows that the S–Mo–S layers are aligned with the (002) basal plane parallel to the substrate. The averaged d_{002} obtained from the TEM

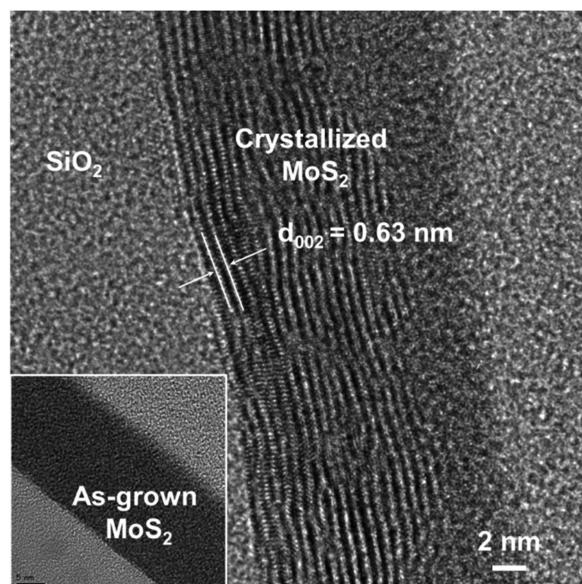

Fig. 6 Cross-sectional high resolution TEM image of the MoS_2 film annealed at 900 °C for 5 min. The TEM image in the inset shows the amorphous nature of the as-grown film.

This journal is © The Royal Society of Chemistry 2014

image is around 0.63 nm, which is also consistent with the d_{002} value obtained by XRD. The crystallization of MoS_2 in the parallel direction of the substrate will be advantageous to prepare electronic devices based on MoS_2 such as transistors. However, since the film is not fully crystallized in its thickness due to the short annealing time (5 min), the crystallization process of the as-grown film should be optimized for the device fabrication.

4 Conclusions

In summary, we propose a novel chemical route for MoS_2 ALD using $Mo(CO)_6$ and DMDS as Mo and S precursors, respectively. $Mo(CO)_6$ is chemically adsorbed to be $Mo(CO)_n$ ($n \leq 5$) in the first-half reaction, and the methylthiolate intermediate from the dissociative chemisorption of DMDS in the second-half reaction may undergo additional decomposition to produce sulfur adatoms, possibly owing to the catalytic effect of the chemisorbed $Mo(CO)_n$. Even though the as-grown film is amorphous due to the low growth temperature (100 °C), it clearly shows the characteristic Raman modes ($E^1{}_{2g}$ and A_{1g}) of MoS_2. The as-grown amorphous MoS_2 may be utilized for catalysis applications such as electrochemical HER. In addition, the crystallized MoS_2 by annealing may be used for the electronic applications, since the annealing process results in crystallization of the (002) basal planes in a parallel direction to the SiO_2/Si substrate.

Acknowledgements

This work was supported by Konkuk University in 2012. The authors thank H. K. Kang and M. K. Cho (Advanced Analysis Center, KIST) for XPS and TEM analyses, respectively.

Notes and references

1 A. K. Geim, *Science*, 2009, **324**, 1530.
2 S. Z. Butler, *et al.*, *ACS Nano*, 2013, **7**, 2898.
3 M. Chhowalla, H. S. Shin, G. Eda, L. J. Li, K. P. Loh and H. Zhang, *Nat. Chem.*, 2013, **5**, 263.
4 Q. H. Wang, K. Kalantar-Zadeh, A. Kis, J. N. Coleman and M. S. Strano, *Nat. Nanotechnol.*, 2012, **7**, 699.
5 J. Yang and H. S. Shin, *J. Mater. Chem. A*, 2014, **2**, 5979.
6 K. F. Mak, C. Lees, J. Hone, J. Shan and T. F. Heinz, *Phys. Rev. Lett.*, 2010, **105**, 136805.
7 K. S. Novoselov, D. Jiang, F. Schedin, T. J. Booth, V. V. Khotkevich, S. V. Morozov and A. K. Geim, *Proc. Natl. Acad. Sci. U. S. A.*, 2005, **102**, 10451.
8 B. Radisavljevic, A. Radenovic, J. Brivio, V. Giacometti and A. Kis, *Nat. Nanotechnol.*, 2011, **6**, 147.
9 S. Das, H. Y. Chen, A. V. Penumatcha and J. Appenzeller, *Nano Lett.*, 2013, **13**, 100.
10 T. F. Jaramillo, K. P. Jorgensen, J. Bonde, J. H. Nielsen, S. Horch and I. Chorkendorff, *Science*, 2007, **317**, 100.
11 Y. Li, H. Wang, W. L. Xie, Y. Liang, G. Hong and H. Dai, *J. Am. Chem. Soc.*, 2011, **133**, 7296.
12 F. Schwierz, *Proc. IEEE*, 2013, **101**, 1567.
13 Y. H. Lee, X. Q. Zhang, W. Zhang, M. T. Chang, C. T. Lin, K. D. Chang, Y. C. Yu, J. T. W. Wang, C. S. Chang, L. J. Li and T. W. Lin, *Adv. Mater.*, 2012, **24**, 2320.
14 Y. Zhan, Z. Liu, S. Najmaei, P. M. Ajayan and J. Lou, *Small*, 2012, **8**, 966.
15 X. Wang, H. Feng, Y. Wu and L. Jiao, *J. Am. Chem. Soc.*, 2013, **135**, 5304.
16 Y. Yu, C. Li, Y. Liu, L. Su, Y. Zhang and L. Cao, *Sci. Rep.*, 2013, **3**, 1866.
17 B. Meyer, *Chem. Rev.*, 1976, **76**, 367.
18 S. M. George, *Chem. Rev.*, 2010, **110**, 111.
19 M. Diskus, O. Nilsen and H. Fjellvag, *J. Mater. Chem.*, 2011, **21**, 705.
20 D. Seghete, G. B. Rayner Jr., A. S. Cavanagh, V. R. Anderson and S. M. George, *Chem. Mater.*, 2011, **23**, 1668.
21 H. Wang, Z. Lu, S. Xu, D. Kong, J. J. Cha, G. Zheng, P. C. Hsu, K. Yan, D. Bradshaw, F. B. Prinz and Y. Cui, *Proc. Natl. Acad. Sci. U. S. A.*, 2013, **110**, 19701.
22 L. K. Tan, B. Liu, J. H. Teng, S. Guo, H. Y. Low and K. P. Loh, *Nanoscale*, 2014, **6**, 10584.
23 C. Yim, M. O'Brien, N. McEvoy, S. Winters, I. Mirza, J. G. Lunney and G. S. Duesberg, *Appl. Phys. Lett.*, 2014, **104**, 103114.
24 T. Ohta, F. Cicoira, P. Doppelt, L. Beitone and P. Hoffmann, *Chem. Vap. Deposition*, 2001, **7**, 33.
25 R. Chellappa and D. Chandra, *J. Chem. Thermodyn.*, 2005, **37**, 377.
26 J. S. Cross and G. L. Schrader, *Thin Solid Films*, 1995, **259**, 5.
27 K. A. Gesheva and T. Ivanova, *Chem. Vap. Deposition*, 2006, **12**, 231.
28 K. Reddy and T. L. Brown, *J. Am. Chem. Soc.*, 1995, **117**, 2845.
29 H. H. Huang, C. S. Sreekanth, C. S. Seet, X. Jiang and G. Q. Xu, *Surf. Sci.*, 1996, **365**, 769.
30 Z. Jiang, L. Xu and X. Huang, *J. Mol. Catal. A: Chem.*, 2009, **304**, 16.
31 P. Kruger, M. Petukhov, B. Domenichini, A. Berko and S. Bourgeois, *J. Phys. Chem. C*, 2012, **116**, 10617.
32 R. G. Nuzzo, B. R. Zegarski and L. H. Dubois, *J. Am. Chem. Soc.*, 1987, **109**, 733.
33 B. C. Wiegand and C. M. Friend, *Chem. Rev.*, 1992, **92**, 491.
34 B. Halevi and J. M. Vohs, *Surf. Sci.*, 2008, **602**, 198.
35 M. G. Roper and R. G. Jones, *Phys. Chem. Chem. Phys.*, 2008, **10**, 1336.
36 F. P. Cometto, V. A. Macagno, P. Parcedes-Olivera, E. M. Patrito, H. Ascolani and G. Zampieri, *J. Phys. Chem. C*, 2010, **114**, 10183.
37 D. M. VonNiederhausern, G. M. Wilson and N. F. Giles, *J. Chem. Eng. Data*, 2006, **51**, 1990.
38 N. T. McDevitt, J. E. Bultman and J. S. Zabinski, *Appl. Spectrosc.*, 1998, **52**, 1160.
39 J. L. Verble and T. J. Wieting, *Phys. Rev. Lett.*, 1970, **25**, 362.

This journal is © The Royal Society of Chemistry 2014

40 C. Lee, H. Yan, L. E. Brus, T. F. Heinz, J. Hone and S. Ryu, *ACS Nano*, 2010, **4**, 2695.
41 G. L. Frey, R. Tenne, M. J. Matthews, M. S. Dresselhaus and G. Dresselhaus, *Phys. Rev. B: Condens. Matter*, 1999, **60**, 2883.
42 A. P. S. Gaur, S. Sahoo, M. Ahmadi, M. J. F. Guinel, S. K. Gupta, R. Pandey, S. K. Dey and R. S. Katiyar, *J. Phys. Chem. C*, 2013, **117**, 26262.
43 Y. S. Min, E. J. Bae, B. S. Oh, D. Kang and W. Park, *J. Am. Chem. Soc.*, 2005, **127**, 12498.
44 E. J. Bae, Y. S. Min, J. H. Ko, D. Kang and W. Park, *Chem. Mater.*, 2005, **17**, 5141.
45 N. T. McDevitt, J. S. Zabinski, M. S. Donley and J. E. Bultman, *Appl. Spectrosc.*, 1994, **48**, 733.
46 D. Merki, S. Fierro, H. Vrubel and X. Hu, *Chem. Sci.*, 2011, **2**, 1262.
47 B. Schonfeld, J. J. Huang and S. C. Moss, *Acta Crystallogr., Sect.B: Struct. Sci.*, 1983, **39**, 404.

 This journal is © The Royal Society of Chemistry 2014